# Workspace Analysis for Parameter Optimization of a Cable-driven Boat Motion Simulator

Joonyoung Jang
Mechanical and Aerospace Engineering Department
University of California, San Diego
San Diego, USA
j7jang@ucsd.edu

Thomas Bewley
Mechanical and Aerospace Engineering Department
University of California, San Diego
San Diego, USA
tbewley@ucsd.edu

Abstract—The cable-driven Boat Motion Simulator is a mechanical system designed to replicate the intricate 6 degrees of freedom motions experienced by a boat. This simulator consists of 8 cables and a moving platform. The platform is connected to the cables, and its position is controlled by actuating motors that adjust the cable lengths accordingly. To accurately replicate the desired boat motions, optimizing the design parameters that offer sufficient workspace for the simulator is crucial. This paper focuses on analyzing the workspace using three design parameters: height, width, and cable attachment points. Examining the workspace under various parameter configurations aims to optimize the design and ensure that the simulator provides a sufficient range of motion to replicate complex boat motions accurately. To assess the workspace, we developed a simulation model and an algorithm incorporating three methods: static equilibrium analysis, cable-to-cable interactions, and cable-toplatform interference detection algorithm. This research provides insights into achieving an optimized design for the Cable-driven Boat Motion Simulator, enabling realistic boat motion replication.

Index Terms—Cable-driven Parallel Robot, Workspace Analysis, Static Analysis, Design Parameter Optimization, Cable Interference

#### I. INTRODUCTION

The Cable-driven parallel robot (CDPR) has a movable platform connected to multiple cables. By manipulating the cable lengths, the platform can be positioned to achieve desired motions. CDPRs are renowned for their ability to deliver high-precision motion, particularly with high accelerations [1]. Furthermore, CDPRs utilize lightweight cables, which reduce inertia and exhibit robustness when subjected to high payloads [2] [3]. Due to their simple and lightweight mechanical structure, CDPRs are widely regarded as suitable solutions for applications that require expansive workspaces, easily adjusting configuration and size [4]. Considering the advantages of CDPRs, we chose the CDPR mechanism to build a boat motion simulator. The simulator aims to mimic the motion of the USS Oliver Hazard Perry-class frigate. Frigate's motion is a 6-DOF motion, including a maximum roll angle of 30 degrees and a sway magnitude of 5 centimeters on a 1/100 scale [5]. Thus, the simulator with eight cables and a platform requires a sufficient range of 6-DOF boat motion.

This research aims to determine the workspace of the cable-driven boat motion simulator, ensuring it can effectively

imitate the desired boat motions by providing a suitable range of motion. Three design parameters were considered: platform height, width, and cable attachment points on the platform. The workspace of the simulator varies based on these parameters, and simulation tests were conducted to optimize these parameters for achieving the desired frigate motions.

We investigated three methods for determining the workspace of the cable-driven boat motion simulator. Firstly, since the simulator consists of eight cables and moves at 6-DOF, it can be classified as an underdetermined system. The tension solutions can be optimized at the equilibrium state with this system [6]. We used Singular Value Decomposition (SVD) on the static equilibrium equation to analyze the tension solutions. The rank of the Structure matrix in the static equation was examined to determine if the underdetermined CDPR has infinite or no solutions [7]. Additionally, as the CDPR incorporates multiple cables, cable-to-cable and cableto-platform interference were considered as they influence the determination of the workspace. Detecting cable-to-cable interference involves calculating the shortest distance between cables. This can be achieved by computing the magnitude of the perpendicular vector formed by two cable vectors obtained by the inverse kinematics [8]. Cable-to-platform interference can be detected when a cable intersects with or passes through the side, upper, or bottom planes of the platform. To detect cable-to-platform interference, the cable attachment vectors are utilized to determine the planes of the platform. By comparing the angle between a cable vector and the neighboring platform plane, it can be determined whether interference occurs. When the angle between a cable vector and the plane of the platform is zero, it indicates that the cable is intersecting or passing through the platform, resulting in interference [9]. Based on these methods, we developed an algorithm to determine the workspace of the cable-driven boat motion simulator. The algorithm incorporated static analysis and interference detection methods. We utilized a simulation model of the boat motion simulator to analyze the workspace and applied the algorithm, providing insights into the achievable workspace and potential interference within the system.

The organization of this paper is as follows. Section II overviews the inverse kinematics and static equilibrium principles of the cable-driven boat motion simulator. In Section

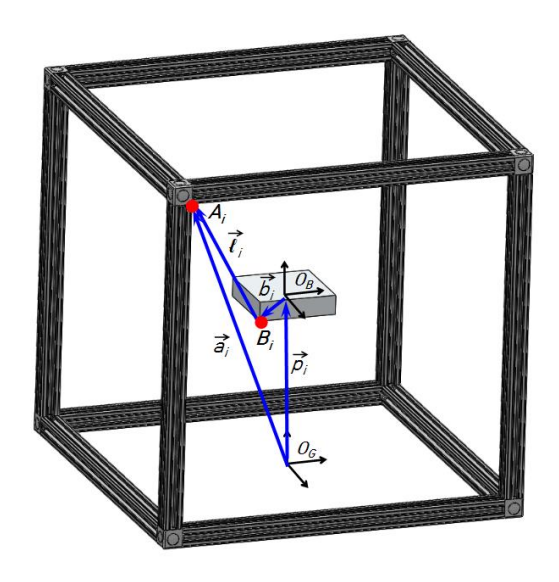


Fig. 1: Configuration of Cable driven boat motion simulator.  $O_G$  and  $O_B$  represent the origins of the global and the platform body frame.  $A_i$  and  $B_i$  are pulley locations on a structure and cable attachment point on a platform of i-th cable relatively.

III, the methods for static analysis and interference detection are discussed. Section IV presents the simulation experiment results of the workspace analysis for design parameter optimization. The results obtained from these experiments can be used to optimize the design for replicating the desired boat motions. Section V concludes the paper by summarizing the obtained results and highlighting the contributions of the study. It also discusses future works, including the construction of a hardware model for experimental tests to validate the results.

#### II. PRELIMINARY

## A. Inverse Kinematics

The inverse kinematics of CDPRs involve calculating cable length vectors and the structure matrix that determines a force vector induced by cable tensions. In Fig. 1 is the configuration of the cable-driven boat motion simulator. The global frame, denoted as  $O_G$  is located in the center of the ground, while the platform body frame,  $O_B$ , is located at the center of the platform.  $\vec{a}_i$  represents the position vector of the pulley for the i-th cable, where  $i = \{1, \cdots, n\}$ , with n being the total number of cables.  $\vec{p} = [x \ y \ z]^T$  represents the position vector of the moving platform in the global frame  $O_G$ . Additionally,  $\vec{b}_i$  is the cable attachment point vector in the body frame  $O_B$ , and R denotes the rotation matrix of the platform in the global frame  $O_G$ . The cable vector defined as  $\vec{l}_i$ , can be determined by inverse kinematics equations [10],

$$\vec{l}_i = \vec{a}_i - R\vec{b}_i - \vec{p}, \quad (i = 1, \dots, n).$$
 (1)

#### B. Static Equilibrium and Structure Matrix

At static equilibrium, the total force exerted by cable tensions is equal to any external forces and moments applied

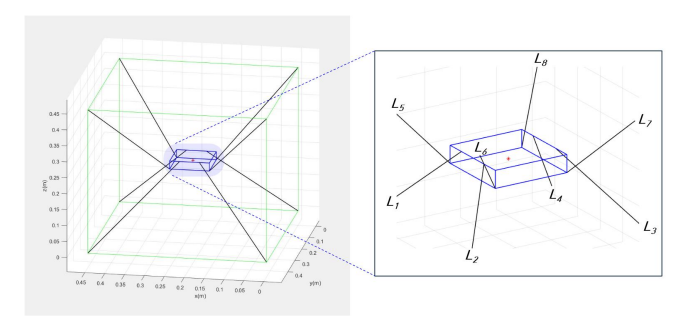


Fig. 2: Cable-driven Boat Motion Simulator simulation model. The green lines represent an outer structure, and eight cables(black) are connected to a moving platform(blue). The figure on the right-hand side provides a zoomed-in perspective of the cables ( $L_1 \sim L_8$ ) and the platform.

to the platform. To achieve the equilibrium, we define the unit cable vector of the *i*-th cable as  $\vec{u}_i = \vec{l}_i/|\vec{l}_i|$ , and the tension vector as  $\vec{\tau}_i = \vec{u}_i|\vec{\tau}_i|$ . Using these definitions, the following equations can be derived [11],

$$\sum_{i=1}^{n} \vec{u}_{i} |\vec{\tau}_{i}| = \vec{F}, \quad \sum_{i=1}^{n} R\vec{b}_{i} \times \vec{u}_{i} |\vec{\tau}_{i}| = \vec{M},$$

where  $\vec{F}$  and  $\vec{M}$  represent the total forces and moments exerted on the platform, respectively. Defining the cable tension vector  $\vec{\tau} = [|\vec{\tau}_1| \cdots |\vec{\tau}_n|]^T$ , the static equation can be written as follows [12],

$$\vec{f} = J\vec{\tau}$$
, with  $J = \begin{bmatrix} \vec{u}_1 & \cdots & \vec{u}_n \\ R\vec{b}_1 \times \vec{u}_1 & \cdots & R\vec{b}_n \times \vec{u}_n \end{bmatrix}_{m \times n}$ ,

where  $\vec{f} = [\vec{F} \ \vec{M}]^T$  is the wrench vector, and m represents the number of degrees of freedom. The Structure matrix, denoted as  $J \in \mathbf{R}^{m \times n}$  is utilized to calculate the tension distribution and perform static analysis [14] [17].

## III. WORKSPACE ANALYSIS METHODS

# A. Static Analysis

Recall the static equilibrium equation formulated as (2), J is a  $m \times n$  matrix where m is DOF, and n is the number of cables connected to a platform. A platform can be positioned where a feasible tension solution is present. The Singular Value Decomposition(SVD) analysis on the Structure matrix J provides insights into identifying feasible solutions. The SVD exists for any matrices, so that matrix J in (2) has an SVD given by  $J = U\Sigma V^T$  where  $U_{m\times m}$  and  $V_{n\times n}$  are unitary matrices, and  $\Sigma_{m\times n}$  is the diagonal matrix with singular values of J,  $\sigma_i$ , on the main diagonal [15]. An SVD of the Structure matrix, J, can be rewritten as follows with r the rank of J [16],

$$\begin{split} J_{m\times n} &= U \Sigma V^T \\ &= \left[ \underline{U}_{m\times r} \quad \overline{U}_{m\times (m-r)} \right] \begin{bmatrix} \underline{\Sigma}_{r\times r} & 0 \\ 0 & 0 \end{bmatrix} \begin{bmatrix} \underline{V}_{n\times r} \quad \overline{V}_{n\times (n-r)} \end{bmatrix}, \end{split}$$

where.

- $\underline{U}$  is the column space, and  $\overline{U}$  is the left null space of J,
- $\underline{V}$  is the row space, and  $\overline{V}$  is the null space of J.

Leveraging the null space of J, such that  $J\overline{V} = 0$ , the tension solution can be written as [17],

$$\vec{\tau} = J^{\dagger} \vec{f} + \overline{V} \vec{h},\tag{4}$$

where  $J^{\dagger}$  is the pseudo inverse matrix of J, and  $\vec{h}$  is an arbitrary vector. Choosing  $\vec{h}$  in (4) yields optimal tension solutions at a specific platform position. Performing an SVD on the matrix J, the (2) can be defined as,

- Underdetermined system with  $\infty$  tension solutions if (n > r = m),
- Both potentially inconsistent and underdetermined systems with  $\infty$  or 0 solutions if (n > r, m > r) depending on  $\vec{f}$ .
- Determined system with only 1 unique tension solution if (m = n = r),
- Overdetermined system with 0 or 1 if (m > r = n) tension solution depending on  $\vec{f}$ .

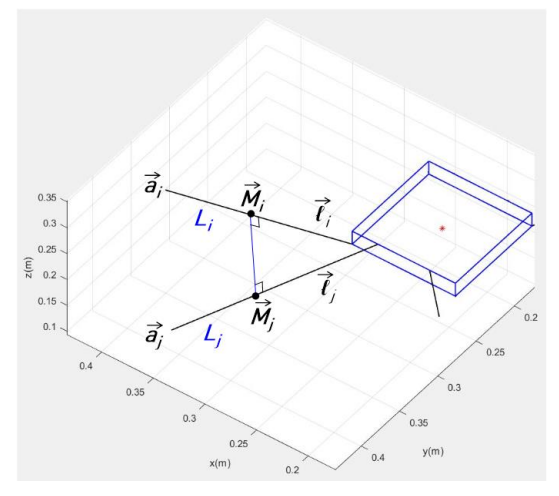
Since the boat motion simulator has eight cables and 6-DOF, it can be defined as an underdetermined system. If J is the full row rank, tension solutions can be infinite, and tension solutions can be optimized. The solution  $\vec{\tau}$  must be a vector of positive tensions to exert forces on a platform since cables can only pull an object and cannot push it [6]. Also, tensions should be minimized because too high tensions can damage the structures or cables. The final solution  $\vec{\tau}$  can be calculated by determining the arbitrary vector  $\vec{h}$  in (4) such that [18],

$$\underset{h}{\operatorname{arg\,min}} \quad \vec{\tau}$$
 subject to 
$$\vec{\tau} = J^{\dagger} \vec{f} + \overline{V} \vec{h}$$
 
$$0 \leq \vec{\tau}$$
 (5)

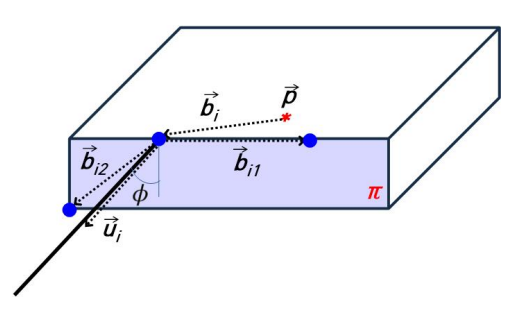
Once the vector  $\vec{h}$  is determined by solving the equation above, it signifies that a platform is located inside the feasible workspace with the tension solution satisfying the condition in (5).

## B. Cable-to-Cable Interference

As depicted in Fig. 2, the upper and lower cables are interconnected to the platform instead of being connected to the platform's edges to expand the rotational workspace. As discussed in III-A, static analysis enables determining tension solutions for a given platform position within the feasible workspace. However, due to the crossing cables, there is interference between cables even inside the feasible workspace. These interferences lead to constraints in the platform's motion and must be discussed to ensure unrestricted movement. Cable-to-cable interference can occur when two cables intersect as the platform moves. By calculating the distance between two cables, it is possible to detect such interference. If the distance between two cables becomes smaller than the diameter of a cable, it indicates an interference between cables. In Fig. 3a,  $\vec{l_i}$  and  $\vec{l_j}$  represent the vectors corresponding to



(a) Cable-to-Cable interference.



(b) Cable-to-Platform interference.

Fig. 3: Interference Detection

cable  $L_i$  and  $L_j$ .  $\vec{a}_i$  and  $\vec{a}_j$  denote the pulley position vector on the outer frame. The vector  $\vec{M}_{ij} = (\vec{M}_i - \vec{M}_j)$  is perpendicular to both cable vectors and  $\vec{M}_i$  and  $\vec{M}_j$  can be defined as follows [8],

$$\vec{M}_i = \vec{a}_i + \lambda_i \vec{u}_i,$$
  
$$\vec{M}_j = \vec{a}_j + \lambda_j \vec{u}_j,$$

where the unit cable vectors are defined as  $\vec{u}_i = \vec{l}_i/|\vec{l}_i|$  and  $\vec{u}_j = \vec{l}_j/|\vec{l}_j|$ .  $\lambda_i$  and  $\lambda_j$  represent the magnitudes of vectors. The cross product  $(\vec{u}_i \times \vec{u}_j)$  is a direction vector of  $\vec{M}_{ij}$ . Given that  $\vec{a}_i$  and  $\vec{a}_j$  are points on lines of  $L_i$  and  $L_j$ , the shortest distance between two cables can be determined by calculating the length of the orthogonal projection of  $(\vec{a}_i - \vec{a}_j)$  on  $\vec{M}_{ij}$ . The formula for this calculation is as follows [19],

$$d_{ij} = \left| \frac{(\vec{a}_i - \vec{a}_j) \cdot (\vec{u}_i \times \vec{u}_j)}{|\vec{u}_i \times \vec{u}_j|} \right|. \tag{6}$$

If  $d_{ij}$  is smaller than the cable diameter  $\epsilon$  ( $d_{ij} \leq \epsilon$ ), it implies the interference between two cables,  $L_i$  and  $L_j$ .

## C. Cable-to-Platform Interference

Fig. 3b illustrates a platform and a cable connected to the attachment point. A vector  $\vec{b}_i$  represents the attachment point vector of the *i*-th cable in the body frame on the platform

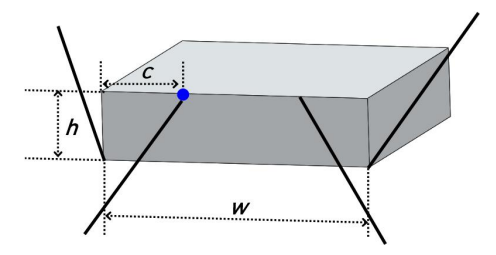


Fig. 4: Design Parameters: The platform height(h), width(w), and the cable attachment point(c).

center p.  $\vec{b}_{i1}$  and  $\vec{b}_{i2}$  are the vectors from the attachment point of i-th cable to the neighboring cable attachment points. Consider the plane  $\pi$  formed by two vectors  $\vec{b}_{i1}$  and  $\vec{b}_{i2}$ , and define  $\phi$  as the angle between  $\pi$  and the unit cable vector  $\vec{u}_i$ . To detect the interference, the perpendicular vector of plane  $\pi$  needed to be defined with given two vectors  $\vec{b}_{i1}$  and  $\vec{b}_{i2}$ . The perpendicular vector  $\vec{q}$  can be calculated by the vector cross-product,

$$\vec{q_i} = \vec{b}_{i1} \times \vec{b}_{i2}$$
.

Note that the angle between  $\vec{q_i}$  and  $\vec{u_i}$  is  $\frac{\pi}{2} - \phi$  and the angle can be formulated utilizing the dot product,

$$\cos(\frac{\pi}{2} - \phi) = \frac{\vec{q}_i \cdot \vec{u}_i}{|\vec{q}_i||\vec{u}_i|},$$
$$\phi = \sin^{-1}\left(\frac{\vec{q}_i \cdot \vec{u}_i}{|\vec{q}_i||\vec{u}_i|}\right).$$

Cable-to-platform interference occurs when the angle  $\phi$  is less than zero.

## IV. SIMULATION SETUP

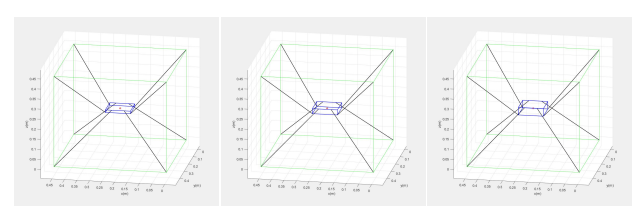
# A. Simulation Model

The configuration of the simulation model for the cable-driven boat motion simulator is illustrated in Fig. 2. The model's outer structure edge size is 45cm, with a platform connected to eight cables. The upper and lower cables are cross-connected, while the lower cables are attached inward from the top edge of the platform.

The simulation test was performed by moving a platform to every position inside the structure. The resolution was 1cm for translation in x, y, and z axis. Based on the desired USS Oliver Hazard class Frigate's motion, eight cases of platform rotation were considered in the test. The sets are roll (0, 30) degrees, pitch (0, 5) degrees, and Yaw (0, 2) degrees, and combinations of rotations are as seen in TABLE I.

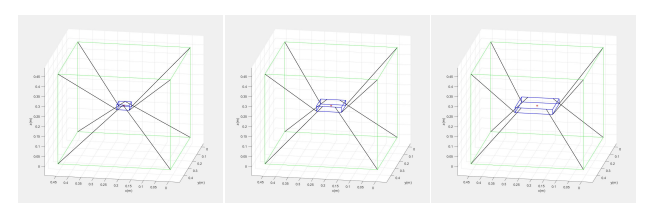
TABLE I: Rotation Motion Test Sets

Case	Roll, Pitch, Yaw	Case	Roll, Pitch, Yaw
1	0, 0, 0	5	30, 0, 0
2	0, 0, 2	6	30, 0, 2
3	0, 5, 0	7	30, 5, 0
4	0, 5, 2	8	30, 5, 2



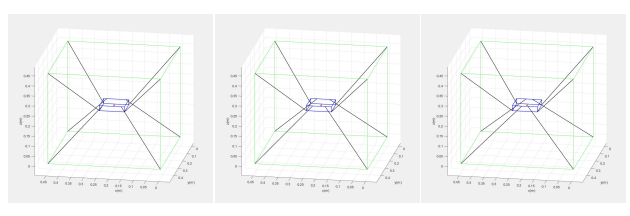
(a) H1: h = 1.25cm (b) D0: h = 2.50cm (c) H2: h = 3.75cm

Fig. 5: Platform Height with w = 10.00cm, c = 2.50cm



(a) W1: w = 5.00cm (b) D0: w = 10.00cm (c) W2: w = 15.00cm

Fig. 6: Platform Width with h = 2.50cm, c = 2.50cm



(a) C1: c = 1.25cm (b) D0: c = 2.50cm (c) C2: c = 3.75cm

Fig. 7: Cable Attachment Point with h = 2.50cm, w = 10.00cm

## B. Design Parameters

Three design parameters were considered during the workspace analysis, as seen in Figure 4. To evaluate the impact of parameter variations, the parameters were modified by decreasing and increasing them by 50 percent from the baseline design denoted as 'D0'.

The first parameter is the platform height, representing the distance between the platform's bottom and top planes. Three different heights were tested to investigate the relationship between platform height and the workspace, as shown in Fig. 5. Design 'D0' is the baseline design with a 2.50cm platform height, while 'H1' has 1.25cm, and 'H2' has 3.75cm.

The second parameter is the platform width, which indicates the space between the edges of the top or bottom plane. Various width dimensions were experimented with to evaluate the influence of platform width on the workspace, as illustrated in Fig. 6. The baseline design 'D0' features a platform width of 10.00cm, while 'H1' has a width of 5.00cm, and 'H2' extends to a width of 15.00cm.

The third parameter is the cable attachment point. The attachment of lower cables to the edges of the upper platform plane, positioned toward the middle of these edges, is aimed at enhancing rotational motion. Denoted as *b* in Fig. 7, the cable attachment point represents the distance from the nodes

to the attachment points. Various attachment point values were tested to investigate the impact on the workspace. As illustrated in Fig. 7, the baseline design 'D0' features a cable attachment point of 2.50cm, while 'H1' has an attachment point of 1.25cm, and 'H2' is characterized by an attachment point of 3.75cm.

By altering these design parameters and their impact on the workspace, we can acquire insights into how height, width, and cable attachment points influence the extent of motion achievable by the cable-driven boat motion simulator. This analysis allows optimizing the design parameters to attain an optimal workspace replicating the intended boat motions.

#### C. Simulation Alogirthm

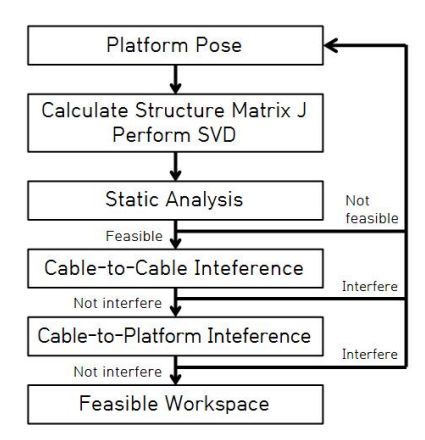


Fig. 8: Simulation test algorithm.

The simulation test was performed with the algorithm shown in Fig. 8. The platform position started from the origin. By (2), (3), the corresponding structure matrix, J, is calculated, and SVD is performed to determine the null space of J. The static analysis investigates the existence of  $\vec{h}$  in (5). If the tension solution is feasible as  $\vec{h}$  exists, the algorithm explores cable-to-cable and cable-to-platform interference utilizing the methods described in III-B,III-C. Finally, the feasible, interference-free platform pose is recorded, and the platform moves to the next pose.

## V. RESULTS

The workspace analysis involves a comparison of the workspace volumes for each design. The outcomes are presented in Table II, which indicates the percentage of feasible workspace occupied by a platform center position to the total number of positions within the structure. The findings reveal that the workspace is most expansive for each design when the platform remains non-rotational and diminishes as rotational motion is introduced. Moreover, it is evident that rotations distinctly influence each design's workspace.

## A. Platform Height

The platform height changes  $(H1 \rightarrow D0 \rightarrow H2)$  exhibit a relatively minor impact on the feasible workspace volume compared to the influences of other parameters. Fig. 9 is

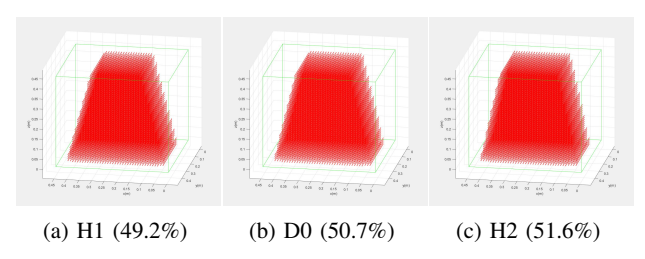


Fig. 9: Case 1 Feasible Workspace (Platform Height)

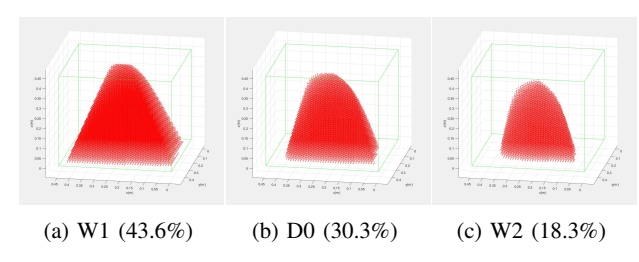


Fig. 10: Case 2 Feasible Workspace (Platform Width)

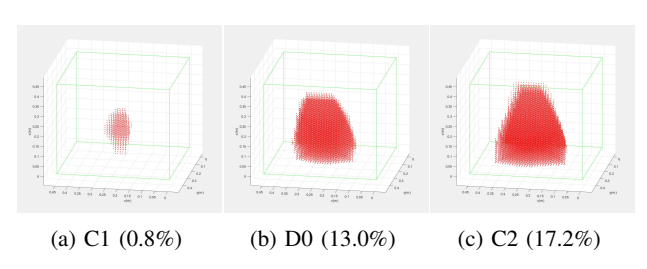


Fig. 11: Case 6 Feasible Workspace (Cable Attachment Point)

TABLE II: Feasible Workspace Volume (%)

Case	D0	H1	H2	W1	W2	C1	C2
1 (0,0,0)	50.7	49.2	51.6	54.6	40.3	50.4	47.1
2 (0,0,2)	30.3	29.7	30.8	43.6	18.3	17.4	34.8
3 (0,5,0)	49.3	47.3	50.8	53.4	39.1	48.9	45.4
4 (0,5,2)	31.5	30.9	31.9	44.7	19.1	18.2	35.8
5 (30,0,0)	16.5	16.9	13.6	26.2	12.9	8.7	18.7
6 (30,0,2)	13.0	12.9	10.8	25.7	6.6	0.8	17.2
7 (30,5,0)	14.7	14.8	11.6	25.6	9.3	1.9	17.8
8 (30,5,2)	15.1	15.1	11.4	25.1	9.7	3.8	18.1

the feasible workspace of Case 1 for designs featuring different heights. The difference between the smallest and largest workspaces ranges from a minimum of 1.0% to a maximum of 3.7%. As the platform height increases, the workspaces for motions without a roll (Case  $1{\sim}4$ ) expand. However, a taller platform negatively affects motions involving a roll (Case  $5{\sim}8$ ) and increases the possibility of cable-to-platform and cable-to-cable interferences.

## B. Platform Width

The variations in platform width  $(W1\rightarrow D0\rightarrow W2)$  have the most substantial impact on the feasible workspace. Changes in platform width lead to a workspace modification ranging from a minimum of 13.3% to a maximum of 25.6%. A smaller platform width is associated with reduced interference

and enhanced tolerance for rotational movements, particularly yaw (Case 2,4,6,8). Fig. 10 visually represents the feasible workspace of Case 2 for each design, highlighting a reduction in workspace volume attributed to yaw motion.

#### C. Cable Attachment Point

As cable attachment points are altered (C1 $\rightarrow$ D0 $\rightarrow$ C2), the feasible workspace undergoes variations ranging from a minimum of 3.3% to a maximum of 17.6%. If the cable attachment point is smaller and positioned close to the corners, the workspace contracts, particularly in the presence of rotations, especially roll. This outcome is due to the increased proximity of two cables at the corners, elevating the possibility of cable-to-cable interference. Fig. 11 illustrates this effect, demonstrating how a larger cable attachment point significantly enlarges the workspace in case 6.

#### VI. CONCLUSION

This research examines the workspace analysis for optimizing the parameters of a Cable-driven Boat Motion Simulator. The study considers three parameters: platform height, width, and cable attachment point, to investigate their impact on the feasible workspace. The results indicate that increasing platform height leads to a smaller workspace when the platform rolls but a larger workspace when a roll is not applied. Platform width significantly affects the workspace, with smaller platforms allowing for a larger feasible workspace in all cases. Also, when the cable attachment point is small and close to the platform's corners, the workspace becomes smaller due to the high chance of cable-to-cable interference. A larger cable attachment point usually results in a larger workspace because the distance between cables is farther. Overall, the findings from simulation tests suggest that smaller platform widths and larger cable attachment points are beneficial for achieving a larger workspace. However, it is essential to consider practical constraints such as platform size providing enough space for electronics and sensors on the platform. Also, there should be sufficient room to perform landing tests for specific applications, like developing an automatic aerial vehicle landing on a moving platform.

Future work will focus on optimizing and determining parameters to ensure an ideal workspace to mimic a boat's motions and conduct further experiments based on the results from this study. Once the optimal parameters are obtained, the hardware prototype model will be built. Moreover, additional simulation tests will be conducted to formulate the relationship between parameters and workspaces more precisely.

#### REFERENCES

- [1] J. Jung, J. Piao, S. Park, J. -O. Park and S. Y. Ko, "Analysis of cable tension of high speed parallel cable robot: High speed position tracking of winch," 2016 16th International Conference on Control, Automation and Systems (ICCAS), Gyeongju, Korea (South), 2016, pp. 1053-1056, doi: 10.1109/ICCAS.2016.7832439.
- [2] J. Jang, M. Zhao and T. Bewley, "A Control Lyapunov Function-Based Quadratic Program for the Cable-Driven Boat Motion Simulator," 2022 7th International Conference on Robotics and Automation Engineering (ICRAE), Singapore, 2022, pp. 18-24, doi: 10.1109/ICRAE56463.2022.10056184.

- [3] R. E. Skelton and M. C. Oliveira, "Tensegrity systems," Springer, 2009.
- [4] J. -A. Seon, S. Park, S. Y. Ko and J. -O. Park, "Cable configuration analysis to increase the rotational range of suspended 6-DOF cable driven parallel robots," 2016 16th International Conference on Control, Automation and Systems (ICCAS), Gyeongju, Korea (South), 2016, pp. 1047-1052, doi: 10.1109/ICCAS.2016.7832438.
- [5] J.L. Sanchez-Lopez, J. Pestana, S. Saripalli, and P. Campoy, "An Approach Toward Visual Autonomous Ship Board Landingof a VTOL UAV," J. Intell. Robotics Syst. 74, 1–2, April 2014, pp. 113–127, doi: https://doi.org/10.1007/s10846-013-9926-3
- [6] J. Jang, and T. Bewley, "Tension optimization of the 6-DOF cabledriven boat motion simulator," RSAE 2021, Paris, France, May 2021, doi: 10.1145/3475851.3475854.
- [7] T. Bewley, "Stabilization of low-altitude balloon systems, Part 2: riggings with multiple taut ground tethers, analyzed as tensegrity systems," University of California, San Diego, 2019, Unpublished.
- [8] M. M. Aref and H. D. Taghirad, "Geometrical workspace analysis of a cable-driven redundant parallel manipulator: KNTU CDRPM," 2008 IEEE/RSJ International Conference on Intelligent Robots and Systems, Nice, France, 2008, pp. 1958-1963, doi: 10.1109/IROS.2008.4650670.
- [9] Dinh Quan Nguyen and Marc Gouttefarde, "On the Improvement of Cable Collision Detection Algorithms," CableCon: Cable-Driven Parallel Robots, Aug 2014, Duisburg, Germany. pp.29-40, doi: 10.1007/978-3-319-09489-2
- [10] S. J. Torres-Mendez, J. R. Mendoza-Vazquez, V. Ramirez-Palacios and I. D. Rojas-Cuevas, "Analytical workspace delineation of a translational underconstrained cable-based robot," 2017 International Conference on Electronics, Communications and Computers (CONIELE-COMP), Cholula, Mexico, 2017, pp. 1-7, doi: 10.1109/CONIELE-COMP,2017.7891812.
- [11] G. Yang, C. B. Pham and S. H. Yeo, "Workspace Performance Optimization of Fully Restrained Cable-Driven Parallel Manipulators," 2006 IEEE/RSJ International Conference on Intelligent Robots and Systems, Beijing, China, 2006, pp. 85-90, doi: 10.1109/IROS.2006.281747.
- [12] X. Diao, "Singularity analysis of fully-constrained cable-driven parallel robots with seven cables," 2015 IEEE International Conference on Mechatronics and Automation (ICMA), Beijing, China, 2015, pp. 1537-1541, doi: 10.1109/ICMA.2015.7237713.
- [13] A. F. Côté, P. Cardou and C. Gosselin, "A tension distribution algorithm for cable-driven parallel robots operating beyond their wrench-feasible workspace," 2016 16th International Conference on Control, Automation and Systems (ICCAS), Gyeongju, Korea (South), 2016, pp. 68-73, doi: 10.1109/ICCAS.2016.7832301.
- [14] Tho, T. P. and Thinh, N. T., "An overview of cable-driven parallel robots: Workspace, tension distribution, and cable sagging. Mathematical Problems in Engineering," July 2022, https://www.hindawi.com/journals/mpe/2022/2199748.
- [15] S. Chen and J. Feng, "Research on detection of fabric defects based on singular value decomposition," The 2010 IEEE International Conference on Information and Automation, Harbin, China, 2010, pp. 857-860, doi: 10.1109/ICINFA.2010.5512449.
- [16] J. Yang, S. Wongsa, V. Kadirkamanathan, S. A. Billings and P. C. Wright, "Metabolic Flux Estimation-A Self-Adaptive Evolutionary Algorithm with Singular Value Decomposition," in IEEE/ACM Transactions on Computational Biology and Bioinformatics, vol. 4, no. 1, pp. 126-138, Jan.-March 2007, doi: 10.1109/TCBB.2007.1032.
- [17] M. Fabritius, G. Rubio-Gómez, C. Martin, J. C. Santos, W. Kraus and A Pott, "A nullspace-based force correction method to improve the dynamic performance of cable-driven parallel robots," Mechanism and Machine Theory, Volume 181, 2023, 105177, ISSN 0094-114X, https://doi.org/10.1016/j.mechmachtheory.2022.105177.
- [18] W. B. Lim, S. H. Yeo and G. Yang, "Optimization of Tension Distribution for Cable-Driven Manipulators Using Tension-Level Index," in IEEE/ASME Transactions on Mechatronics, vol. 19, no. 2, pp. 676-683, April 2014, doi: 10.1109/TMECH.2013.2253789.
- [19] M. A. Carpio-Alemán et al., "Collision and Tension Analysis of Cable-Driven Parallel Robot for Positioning and Orientation," 2018 IEEE International Autumn Meeting on Power, Electronics and Computing (ROPEC), Ixtapa, Mexico, 2018, pp. 1-6, doi: 10.1109/ROPEC.2018.8661464.